Manuscript ID: jp-2011-043174 (Revised)

Permanganate Oxidation of α-Amino Acids: Kinetic Correlations for the Non-Autocatalytic and Autocatalytic Reaction Pathways

Joaquin F. Perez-Benito*

Departamento de Quimica Fisica, Facultad de Quimica, Universidad de Barcelona, Marti i Franques, 1, 08028 Barcelona, Spain

* Fax: 34 93 4021231. E-mail: jfperezdebenito@ub.edu.

Abstract

The reactions of permanganate ion with seven α-amino acids in aqueous KH_2PO_4-K_2HPO_4 buffers have been followed spectrophotometrically at two different wavelengths: 526 nm (decay of MnO_4^-) and 418 nm (formation of colloidal MnO_2). All the reactions studied were autocatalyzed by colloidal MnO_2, the contribution of the autocatalytic reaction pathway decreasing in the order glycine > L-threonine > L-alanine > L-glutamic acid > L-leucine > L-isoleucine > L-valine. The rate constants corresponding to the non-autocatalytic and autocatalytic pathways have been obtained by means of either a differential rate law or an integrated one, the latter requiring the use of an iterative method for its implementation. The activation parameters for the two pathways have been determined and analyzed in order to obtain statistically significant correlations for the series of reactions studied. The activation enthalpy of the non-autocatalytic pathway showed a strong, positive dependence on the standard Gibbs energy for the dissociation of the protonated amino group of the α-amino acid. Linear enthalpy-entropy correlations were found for both pathways, leading to isokinetic temperatures of 370 ± 21 K (non-autocatalytic) and 364 ± 28 K (autocatalytic). Mechanisms in agreement with the experimental data are proposed for the two reaction pathways.

Introduction

Autocatalysis is an important phenomenon in both the chemical and biological fields because it plays a key role in the mechanism of oscillating processes, such as the much studied Belousov-Zhabotinsky reaction,[1] and in life-related feed-back cycles, as the ones involved in the dynamics of pattern formation in biomimetic systems,[2] in the evolution of homochirality,[3,4] and in molecular replication and the origin of life.[5,6]

Potassium permanganate is one of the most versatile oxidants and has been utilized extensively in acid, alkaline, and neutral media for the oxidation of organic compounds.[7,8] The kinetics of the oxidations of α-amino acids by permanganate ion in both acid[9-26] and neutral[27-41] media has received considerable attention in the last decades. For instance, the permanganate oxidation of glycine in the presence of phosphoric acid has been reported to show an oscillating behaviour.[42] Another important aspect of these reactions is that they usually yield rate-time plots showing autocatalytic profiles, observed in both acid and neutral solutions. Although the acceleration can usually be detected from the beginning of the reactions, in the case of acid solutions a phenomenon of delayed autocatalysis has been reported.[43-46] Whereas the autocatalysis found in acid media can be explained by the joint contributions of the Mn(II) ion formed as a reaction product (acting as a reducing agent for permanganate ion) and the colloidal Mn(IV) formed as a long-lived intermediate (acting as a heterogeneous catalyst for the reaction), that found in neutral media can be explained by the sole contribution of the colloidal Mn(IV) formed as the autocatalytic reaction product. This interpretation of the nature of the autocatalysts is consistent with the finding that the permanganate oxidations of organic substrates in alkaline media, where the inorganic product is Mn(VI) and lower oxidation states [from Mn(IV) to Mn(II)] are not expected to be involved in the mechanism neither as intermediates or reaction products, present no observable

autocatalysis.[47,48] Conversely, in the permanganate oxidation of oxalic acid in aqueous sulfuric media autocatalysis has been reported to be caused by the lower oxidation states of manganese, the long-lived intermediate colloidal Mn(IV) playing a crucial role in the mechanism of the autocatalytic reaction pathway.[49]

When the permanganate oxidations of organic compounds are performed in phosphate-buffered aqueous solutions the reaction rate can be notably affected by the concentration of phosphate ions in different ways. This happens in the oxidations of the α-amino acid glycine and of the biocide triclosan, both of them autocatalytic, but, whereas in the first case phosphate ions inhibit the autocatalytic pathway,[50] in the second case these ions enhance the global reaction rate.[51,52]

Given the importance of autocatalytic processes, and the relative scarcity of reliable kinetic data for autocatalytic reactions, in the present work an effort has been made to establish some kinetic relationships between the activation parameters corresponding to the non-autocatalytic and autocatalytic reaction pathways for the permanganate oxidation of seven different α-amino acids in neutral aqueous solutions. Although in acid media it has been reported that α-amino acids with an even number of carbon atoms in the side chain have a different reactivity toward permanganate from those with an odd number of carbon atoms,[53,54] this complex, dual behaviour has not been confirmed by the kinetic data now presented in neutral solution. The results found allow us to conclude that the reactions studied, whose general stoichiometry is:

$$2MnO_4^- + 3NH_3^+CHRCO_2^- + 2H^+ = 2MnO_2 + 3NH_3 + 3RCHO + 3CO_2 + H_2O \quad (1)$$

share a common mechanism, and plausible proposals are made for the sequences of elementary steps followed by the two oxidation pathways.

Experimental Section

Materials and Instruments. The solvent was twice-distilled water. All the reactants ($KMnO_4$, glycine, L-alanine, L-threonine, L-valine, L-glutamic acid, L-leucine, L-isoleucine, KH_2PO_4, and $K_2HPO_4 \cdot 3H_2O$) were of analytical-grade quality (Merck). The chemical structures corresponding to the seven α-amino acids acting in the present study as reducing agents are shown in Table 1, and all of them were used in large excess with respect to the oxidant, potassium permanganate. A KH_2PO_4-K_2HPO_4 buffer mixture was used in all the experiments. The pH measurements were done with a Metrohm 605 pH-meter provided with a glass-calomel combined electrode. The kinetic runs were followed with a Varian Cary 219 spectrophotometer, using thermostatized glass cells (optical-path length 1 cm), and measuring both the decay of MnO_4^- at 526 nm and the formation of colloidal MnO_2 at 418 nm. The UV-vis spectra were recorded using quartz cells of the same optical-path length.

Kinetic Method. The values of the permanganate concentration at different instants during each kinetic run were obtained from the absorbances at 526 nm (wavelength at which permanganate ion presents an absorption maximum) and 418 nm (wavelength at which permanganate ion is almost transparent to radiation) by means of the equation:

$$[MnO_4^-]_t = \frac{A(526)_t - [\varepsilon_P(526)/\varepsilon_P(418)]A(418)_t}{\varepsilon_R(526)l} \quad (2)$$

where the numbers in parenthesis indicate wavelengths, ε_R and ε_P are the molar absorption coefficients of the reactant (MnO_4^-) and product (colloidal MnO_2), respectively, whereas l is the optical-path length. The reaction rates at different instants during the course of the reaction

were obtained from the permanganate concentration data by the finite-increment approximate derivation method:

$$v = - \frac{d[MnO_4^-]_t}{dt} \approx - \frac{\Delta c}{\Delta t} \quad (3)$$

applied at short time intervals, where c stands for the permanganate concentration at time t.

Statistical Method. The validity of the different kinetic correlations attempted for the series of seven reactions studied was either confirmed or disproved by means of the analysis of variance (ANOVA) method, leading to the value of the probability of a particular correlation being due to hazardous errors (P). A correlation (either straight line or curve) was considered statistically significant when $P < 0.05$.

Results

Kinetic Plots. For some α-amino acids and under certain experimental conditions the absorbance vs time plots showed the usual upward-concave (at 526 nm) or downward-concave (at 418 nm) curvature expected for kinetic plots corresponding to either non-autocatalytic or only slightly autocatalytic reactions. In many experiments, however, it was possible to observe the Z-shaped (at 526 nm, Figure 1, top) and S-shaped (at 418 nm, Figure 1, bottom) sigmoidal curves characteristic of autocatalytic reactions. In the latter cases the reaction rate vs time plots showed a bell-shaped profile (Figure 2, top).

Kinetic Equations. The reaction rate (v) - permanganate concentration (c) experimental data for most autocatalytic permanganate reactions are consistent with the differential rate law:

$$v = k_1 c + k_2 c (c_o - c) \quad (4)$$

where k_1 and k_2 are the pseudo-first-order and pseudo-second-order rate constants (the α-amino acids were in large excess) of the non-autocatalytic and autocatalytic reaction pathways, respectively, whereas c_o is the initial permanganate concentration.[55]

Integration of eq 4 leads to:

$$\ln \frac{k_1 + k_2 (c_o - c)}{c} = \ln \frac{k_1}{c_o} + (k_1 + k_2 c_o) t \qquad (5)$$

This integrated rate law was used by means of an iterative method until convergence in the values of k_1 and k_2 was achieved. Equation 5 yielded good linear plots for the permanganate oxidations of all α-amino acids studied with the exception of glycine, for which an important systematic deviation from the theoretical differential (eq 4) and integrated (eq 5) rate laws was observed. For this latter case the values of both k_1 and k_2 were obtained from the tangents to the v/c vs c curves at time zero,[50] since according to eq 4, a v/c vs c plot should be linear with a negative slope (- k_2).

Rate Constants. In a typical plot for the oxidation of L-threonine the linearity of an ln $[(k_1 + k_2 c_o - k_2 c) / c]$ vs time plot (eq 5) was excellent up to 50% of progression of the reaction, and a slight downward-concave curvature could be observed after the maximum rate was reached (Figure 2, bottom). This deviation was more neatly visualized when the v/c ratio was represented against c (Figure 3). The values for the rate constants k_1 and k_2 obtained for this experiment from the differential (v/c vs c plot) and integrated (ln $[(k_1 + k_2 c_o - k_2 c) / c]$ vs t plot) methods can be compared in Table 2.

Both the non-autocatalytic and the autocatalytic reaction pathways showed base catalysis for all the seven reactions studied, as indicated by an increase of rate constants k_1

and k_2 when the pH of the medium increased. The experimental data for the dependencies of k_1 and k_2 on the concentration of hydrogen ion could be fitted to the equations:

$$\left(1 + \frac{K_{a,1}}{[H^+]}\right) k_1 = \left(k_{a,1} + \frac{k_{b,1}\, K_{a,1}}{[H^+]}\right) [NH_3^+CHRCO_2^-]_T \quad (6)$$

$$\left(1 + \frac{K_{a,2}}{[H^+]}\right) k_2 = \left(k_{a,2} + \frac{k_{b,2}\, K_{a,2}}{[H^+]}\right) [NH_3^+CHRCO_2^-]_T \quad (7)$$

where $K_{a,1}$ and $K_{a,2}$ are the acidity equilibrium constants for the dissociation of the α-amino acid, $k_{a,1}$ and $k_{a,2}$ the rate constants for the acid-catalyzed pathway, and $k_{b,1}$ and $k_{b,2}$ the rate constants for the base-catalyzed pathway corresponding to the non-autocatalytic and autocatalytic reactions, respectively. The values of parameters $K_{a,1}$ and $K_{a,2}$ were optimized so that the linearity of the $(1 + K_{a,1}/[H^+])\, k_1$ vs $1/[H^+]$ (Figure 4, bottom) and $(1 + K_{a,2}/[H^+])\, k_2$ vs $1/[H^+]$ (Figure 4, top) plots was maximal.

The experimental values obtained for the parameters involved in eqs 6 and 7 in the case of the oxidation of L-threonine are shown in Table 3. From these values, the relative contributions of the acid-catalyzed and base-catalyzed pathways for both the non-autocatalytic (Figure 5, bottom) and the autocatalytic (Figure 5, top) reactions have been evaluated for the pH range (6.13-7.53) studied in these experiments. We can see that for the non-autocatalytic reaction both the acid-catalyzed and base-catalyzed pathways had important contributions in that pH range, the contributions being equal at pH 6.93. However, for the autocatalytic reaction the contribution of the base-catalyzed pathway was very predominant, and an extrapolation of the experimental data indicated that the contributions of the acid-catalyzed and base-catalyzed pathways would be equal at an estimated pH of 5.70.

Activation Parameters. The values of of k_1 and k_2 measured at different temperatures (25.0 - 45.0 ºC) fulfilled both the Arrhenius and Eyring equations. Typical examples are

shown in Figure 6 for the oxidation of L-threonine. From the latter, the standard activation enthalpies and entropies corresponding to each reaction pathway were obtained (Table 4).

The activation enthalpy for the non-autocatalytic reaction pathway showed a strong, positive linear dependence on the standard Gibbs energy[56] for the dissociation of the protonated amino group of the corresponding α-amino acid (Figure 7) that was statistically significant (P = 0.0006). However, a similar correlation for the autocatalytic reaction pathway yielded a straight line that was not statistically significant (P = 0.2312).

Isokinetic Relationships. An isokinetic correlation (T_{iso} = 290 K) has been reported for the non-autocatalytic reaction pathway (but not for the autocatalytic one) in the permanganate oxidation of three α-amino acids (glycine, L-alanine and L-phenylalanine) in neutral solution.[57]

In the present study, statistically significant enthalpy-entropy linear correlations were obtained for both the non-autocatalytic (Figure 8, P = 0.00008) and autocatalytic (Figure 9, P = 0.0002) reaction pathways, their slopes leading to isokinetic termperatures of 370 ± 21 K and 364 ± 28 K, respectively.

Relative Contribution of the Autocatalytic Pathway. The percentage of the overall reaction corresponding to the autocatalytic pathway can be calculated as:

$$(\mathrm{PC})_2 = \frac{100}{c_o}\int_0^{c_o} \frac{k_2\, c\,(c_o - c)}{k_1\, c + k_2\, c\,(c_o - c)}\,\mathrm{d}c \tag{8}$$

leading to the result:

$$(\mathrm{PC})_2 = 100\left[1 - \frac{k_1}{k_2\, c_o}\ln\left(1 + \frac{k_2\, c_o}{k_1}\right)\right] \tag{9}$$

It can be inferred from eq 9 that the relative contribution of the autocatalytic reaction pathway increases as the initial concentration of the limiting reactant (c_o) increases. At

$[KMnO_4]_o = 5.00 \times 10^{-4}$ M, pH 6.78 and 25.0 ºC the value of $(PC)_2$ for the different α-amino acids was in the range 21% (L-valine) – 86% (glycine) and was strongly, negatively correlated with the value of the activation enthalpy of the autocatalytic reaction pathway (Figure 10, top). Whereas that statistically-significant plot (P = 0.0002) showed a downward-concave curvature, a correlation of the logarithm of the ratio between the rate constants of the autocatalytic and non-autocatalytic pathways with the activation enthalpy of the autocatalytic reaction pathway led to a straight line with a negative slope (Figure 10, bottom) that was also statistically significant (P = 0.0002).

Discussion

Interpretation of the Kinetic Plots. The finding that the absorbance vs time plots were sigmoidal (and the reaction rate vs time plots bell-shaped) only for some α-amino acids, and under certain experimental conditions, can be explained by simple mathematical methods. By derivation with respect to the permanganate concentration in eq 4, followed by application of the maximum-existence condition (at $c < c_o$), it can be easily deduced that a maximum in the reaction-rate plots can be observed only when:

$$k_2 > \frac{k_1}{c_o} \tag{10}$$

that is, when the relative contribution of the autocatalytic pathway is important enough to compensate the decrease in the reaction rate caused by the decay of the reactant in defect (permanganate ion). If this condition is not fulfilled, the rate plots still have a maximum in a purely mathematic sense, provided that the reaction is autocatalytic, but it cannot be observed

because it would appear at $c > c_o$ (that is, at $t < 0$). From eq 10 it can be easily inferred that it is always possible to observe bell-shaped rate profiles for autocatalytic reactions ($k_2 > 0$) simply by increasing enough the value of c_o.

The slight downward-concave curvature observed in some ln $[(k_1 + k_2\, c_o - k_2\, c) / c]$ vs t (Figure 2, bottom) or v/c vs c (Figure 3) plots is consistent with a decrease in the activity of the autocatalytic product MnO_2 while the reaction advances as a consequence of the increase in size of its colloidal particles, either by flocculation or by the autocatalytic reaction taking place on their surface and depositing more MnO_2, thus decreasing the specific active area per molecule of autocatalyst.

Mechanism of the Non-autocatalytic Pathway. In agreement with the experimental data, the following mechanism can be proposed for the MnO_2-independent reaction pathway:

$$NH_3^+CHRCO_2^- \underset{}{\overset{K_I}{\rightleftharpoons}} NH_2CHRCO_2^- + H^+ \qquad (11)$$

$$MnO_4^- + NH_3^+CHRCO_2^- \xrightarrow{k_{II}} HMnO_4^- + NH^{\cdot}CHRCO_2^- + H^+ \qquad (12)$$

$$MnO_4^- + NH_2CHRCO_2^- \xrightarrow{k_{III}} HMnO_4^- + NH^{\cdot}CHRCO_2^- \qquad (13)$$

$$MnO_4^- + NH^{\cdot}CHRCO_2^- \longrightarrow MnO_4^{2-} + NH{=}CHR + CO_2 \qquad (14)$$

$$MnO_4^{2-} + H^+ \rightleftharpoons HMnO_4^- \qquad (15)$$

$$HMnO_4^- + NH_2CHRCO_2^- \longrightarrow H_2MnO_4^{2-} + NH{=}CHR + CO_2 \qquad (16)$$

$$NH{=}CHR + H_2O \longrightarrow NH_3 + RCHO \qquad (17)$$

$$H_2MnO_4^{2-} + H^+ \longrightarrow MnO_2 + H_2O + HO^- \qquad (18)$$

$$n\, MnO_2 \longrightarrow (MnO_2)_n \qquad (19)$$

If we assume that eqs 12 and 13 are slow enough to be the rate-determining steps corresponding to the acid-catalyzed and base-catalyzed pathways of the non-autocatalytic reaction, respectively, the proposed mechanism yields the following rate law for this reaction:

$$v_1 = \frac{(k_{II}\,[H^+] + K_I\,k_{III})\,[MnO_4^-]\,[NH_3^+CHRCO_2^-]_T}{K_I + [H^+]} \quad (20)$$

and for its associated pseudo-first-order rate constant:

$$k_1 = \frac{(k_{II}\,[H^+] + K_I\,k_{III})\,[NH_3^+CHRCO_2^-]_T}{K_I + [H^+]} \quad (21)$$

where $[NH_3^+CHRCO_2^-]_T = [NH_3^+CHRCO_2^-] + [NH_2CHRCO_2^-]$ is the total concentration of α-amino acid (both the zwitterionic and basic forms included). Equation 20 is consistent with the experimental information available for the non-autocatalytic reaction pathway: kinetic orders unity for permanganate ion and α-amino acid, as well as base catalysis (Figure 4, bottom).[58]

Theoretical eq 21 is consistent with experimental eq 6 if equilibrium constant $K_{a,1} = K_I$, and rate constants $k_{a,1} = k_{II}$ and $k_{b,1} = k_{III}$. The value obtained in the present kinetic study for the equilibrium constant associated to eq 11 in the case of L-threonine ($pK_{a,1} = 8.20 \pm 0.04$, Table 3) is consistent with the value reported in the literature for the dissociation of the ammonium group of the zwitterionic form of that α-amino acid ($pK_a = 9.10$ at zero ionic strength[56]) if we allow for the increase in the value of the equilibrium constant (and decrease in pK_a) as the ionic strength increases expected for a reaction whose reverse process involves two unlike-charged species (eq 11). Moreover, the finding that the non-autocatalytic pathway

for this family of reactions shows base catalysis implies that the rate constant associated to the oxidation of the basic form of the α-amino acid (eq 13) be higher than that corresponding to the zwitterionic form (eq 12) [in the case of L-threonine $k_{III} = (19 \pm 3)\ k_{II}$, Table 3]. This fact can be easily explained by the higher electron density on the nitrogen atom of the basic form.

Mechanism of the Autocatalytic Pathway. According to the experimental data, the following mechanism can be proposed for the MnO_2-dependent reaction pathway:

$$(MnO_2)_n + NH_3^+CHRCO_2^- \overset{K_{IV}}{\rightleftharpoons} (MnO_2)_n{-}NH_3^+CHRCO_2^- \quad (22)$$

$$(MnO_2)_n{-}NH_3^+CHRCO_2^- \overset{K_V}{\rightleftharpoons} (MnO_2)_n{-}NH_2CHRCO_2^- + H^+ \quad (23)$$

$$(MnO_2)_n{-}NH_3^+CHRCO_2^- + MnO_4^- \xrightarrow{k_{VI}} HMnO_2{-}(MnO_2)_{n-1} + NH{=}CHR + CO_2 + HMnO_4^- \quad (24)$$

$$(MnO_2)_n{-}NH_2CHRCO_2^- + MnO_4^- \xrightarrow{k_{VII}} HMnO_2{-}(MnO_2)_{n-1} + NH{=}CHR + CO_2 + MnO_4^{2-} \quad (25)$$

$$NH{=}CHR + H_2O \longrightarrow NH_3 + RCHO \quad (26)$$

$$HMnO_2{-}(MnO_2)_{n-1} + MnO_4^- \longrightarrow (MnO_2)_n + HMnO_4^- \quad (27)$$

$$MnO_4^{2-} + H^+ \rightleftharpoons HMnO_4^- \quad (28)$$

$$HMnO_4^- + NH_2CHRCO_2^- \longrightarrow H_2MnO_4^{2-} + NH{=}CHR + CO_2 \quad (29)$$

$$H_2MnO_4^{2-} + H^+ \longrightarrow MnO_2 + H_2O + HO^- \quad (30)$$

$$(MnO_2)_n + MnO_2 \longrightarrow (MnO_2)_{n+1} \quad (31)$$

If we assume that eqs 24 and 25 are slow enough to be the rate-determining steps corresponding to the acid-catalyzed and base-catalyzed pathways of the autocatalytic reaction, respectively, the proposed mechanism yields the following rate law for this reaction:

$$v_2 = \frac{K_{IV}\,(k_{VI}\,[H^+] + K_V\,k_{VII})\,[MnO_4^-]\,[MnO_2]\,[NH_3^+CHRCO_2^-]_T}{(1 + K_{IV}\,[NH_3^+CHRCO_2^-]_T)\,(K_V + [H^+])} \quad (32)$$

and for its associated pseudo-second-order rate constant:

$$k_2 = \frac{K_{IV}\,(k_{VI}\,[H^+] + K_V\,k_{VII})\,[NH_3^+CHRCO_2^-]_T}{(1 + K_{IV}\,[NH_3^+CHRCO_2^-]_T)\,(K_V + [H^+])} \quad (33)$$

Equation 32 is consistent with the experimental information available for the autocatalytic reaction pathway: kinetic orders unity for permanganate ion and colloidal manganese dioxide, a fractionary order for the α-amino acid, and base catalysis (Figure 4, top).[58]

Theoretical eq 33 is consistent with experimental eq 7 if equilibrium constant $K_{a,2} = K_V$, and rate constants $k_{a,2} = K_{IV}\,k_{VI} / (1 + K_{IV}\,[NH_3^+CHRCO_2^-]_T)$ and $k_{b,2} = K_{IV}\,k_{VII} / (1 + K_{IV}\,[NH_3^+CHRCO_2^-]_T)$. The value obtained in the present kinetic study for the equilibrium constant associated to eq 23 in the case of L-threonine ($pK_{a,2}$ = 7.98 ± 0.01, Table 3) is slightly lower than that obtained for the non-autocatalytic reaction ($pK_{a,1}$ = 8.20 ± 0.04). This might mean that activation by the colloidal MnO_2 particles results in a slight enhancement of the acidity of the zwitterionic form of the α-amino acid. Moreover, the finding that this family of reactions shows base catalysis, not only as far as the non-autocatalytic pathway is concerned, but also in the autocatalytic pathway implies that the rate constant associated to the oxidation of the basic form of the α-amino acid (eq 25) be higher than that corresponding

to the zwitterionic form (eq 24). The difference seems to be much more notable in the case of the autocatalytic reaction [for L-threonine $k_{VII} = (189 \pm 66)\ k_{VI}$, Table 3] than in the case of the non-autocatalytic one [$k_{III} = (19 \pm 3)\ k_{II}$], in consonance with the finding that the contribution of the acid-catalyzed pathway is negligible in the case of the autocatalytic reaction (Figure 5, top) but not in that of the non-autocatalytic one (Figure 5, bottom).

The main difference between the mechanism given in eqs 22-31 and the one usually proposed for the autocatalytic reaction pathway in the permanganate oxidation of α-amino acids in neutral solution is that the organic substrate, after being adsorbed on the autocatalyst surface (eq 22), reduces simultaneously Mn(VII) to Mn(VI) and Mn(IV) to Mn(III) (eqs 24 and 25). This new proposal is consistent with the detection of a small peak at 480 nm, indicative of formation of a long-lived Mn(III) species, in the spectrum of the reaction products obtained from the permanganate-glycine reaction in neutral solution. This peak could only be detected when the reaction was carried out at high concentrations of phosphate buffer, showing up as a small shoulder in the spectrum corresponding to colloidal MnO_2 (Figure 11, bottom), but it could easily be highlighted when the contribution expected from light scattering by the colloid particles (absorbance decreasing with the fourth power of the wavelength, according to Rayleigh's law[59]) was discounted (Figure 11, inset). Then the uv-vis spectrum showed two absorption peaks, one at 275 nm [characteristic of the electronic spectrum of Mn(IV)[60]] and the other at 480 nm [characteristic of the electronic spectrum of Mn(III) [61]] (Figure 11, top). Stabilization of this Mn(III) species in a degree enough to be spectrophotometrically detected could presumably be caused by its chemical bonding to the MnO_2 molecules belonging to the colloidal-particle surface.

Interpretation of the Kinetic Correlations. The finding of a statistically-significant correlation between the standard activation enthalpies of the non-autocatalytic reaction pathway and the standard Gibbs energies for the dissociation of the protonated amino group

of the respective α-amino acids (Figure 7), whereas the corresponding correlation for the autocatalytic reaction pathway was not statistically significant, is consistent with the proposed mechanisms, since the more active reducing agent is in the first case the basic form of the α-amino acid (eq 13) whereas in the second the zwitterionic form is the one involved in a key step as is adsorption of the organic substrate on the colloidal MnO_2 particles (eq 22). The protonated form of the amino group might be required in the autocatalytic pathway to favour the approach of the α-amino acid to the hydroxide-ion groups bound to the colloid surface,[62] which might be the active sites for the adsorption process. On the contrary, phosphate ions are known to inhibit the reaction taking place at the colloid surface, probably because it is the acidic ion ($H_2PO_4^-$) instead of the basic one (HPO_4^{2-}) the buffer ion that is more efficiently bound to colloidal MnO_2.[50]

The linear enthalpy-entropy correlations found for the non-autocatalytic (Figure 8) and autocatalytic (Figure 9) reaction pathways were strongly significant from the purely statistical point of view. However, it is well known that the existence of experimental errors in the values of the rate constants determined at different temperatures tends to produce that kind of linear plots, simply because both the activation enthalpy and the activation entropy for each reaction are obtained from the same ln (k/T) vs $1/T$ plot, so that the error in the activation enthalpy is linearly, positively correlated with the error in the activation entropy.[63,64] As a consequence, much has been discussed on whether the enthalpy-entropy compensation effect (a linear enthalpy-entropy correlation with a positive slope) is caused by a real physico-chemical phenomenon or simply by a statistical correlation of experimental errors.[65-67]

Nevertheless, in the present case the correlations found might have a real physico-chemical cause considering that enthalpy-entropy linear plots derived from statistically-correlated experimental errors are expected to yield slopes very close to the harmonic mean of the experimental temperatures (T_{hm}),[68] whereas the isokinetic temperatures (T_{iso}) obtained

from the slopes of the activation enthalpy-entropy linear plots for both the non-autocatalytic and autocatalytic reaction pathways are somehow higher than T_{hm} (308 K) even when their respective experimental uncertainties are taken into account. This was confirmed by the finding of statistically-significant activation enthalpy-Gibbs energy linear correlations for both the non-autocatalytic (P = 0.0108) and autocatalytic (P = 0.0371) reaction pathways, since it has been demonstrated that the estimates of the activation enthalpy and the activation Gibbs energy (determined at T_{hm}) are not statistically correlated.[69] The isokinetic temperature can be calculated in this case as:

$$T_{iso} = \frac{T_{hm}\, s}{s - 1} \tag{34}$$

where s is the slope of the activation enthalpy-Gibbs energy linear plot. However, a net decrease in the statistical significance of the correlations was observed when the enthalpy-entropy plane was replaced by the enthalpy-Gibbs energy one. A linear plot in the latter plane with $T_{iso} > T_{hm}$ has also been reported for the oxidation of a series of *m*- and *p*-substituted cinnamic acids in methylene chloride solutions by quaternary ammonium permanganate.[70] These linear plots seem to confirm the existence of a real compensation effect in some series of permanganate reactions involving chemically-correlated organic reducing agents.

Although the interpretation of this phenomenon is not clear, since a number of different theories have been proposed in order to explain it,[71-78] one should keep in mind that a purely thermodynamic explanation of the compensation effect cannot be excluded [a shift in the rate-determining step corresponding to a member of the series of reactions toward a more loosely bonded activated complex (because of the introduction of a certain substituent in one of the reactants) would simultaneously cause an increase in both the activation enthalpy and the activation entropy of the reaction].

The finding that the standard activation enthalpies corresponding to the autocatalytic pathway were much higher (and the percentage of the overall reaction corresponding to that pathway much lower) for the reactions of L-leucine, L-isoleucine, and L-valine than for those of the other four α-amino acids (Figure 10) suggests that the presence of a branched side chain represents an obstacle for the autocatalytic pathway to take place, probably by the involvement of a steric-hindrance effect on the adsorption process caused by the methyl group in the C(1) or C(2) positions of the side chain. Moreover, the fact that the lowest standard activation enthalpy and highest percentage of the overall reaction were found for the autocatalytic pathway corresponding to the α-amino acid with the smallest side chain (glycine) seems to confirm that steric hindrance might play an important role in the adsorption of the different α-amino acids on the surface of the colloidal MnO_2 particles.

References and Notes

(1) Taylor, A. F. *Prog. React. Kinet. Mech.* **2002**, *27*, 247.

(2) Rossi, F.; Ristori, S.; Rustici, M.; Marchettini, N.; Tiezzi, E. *J. Theor. Biol.* **2008**, *255*, 404.

(3) Blackmond, D. G. *Proc. Natl. Acad. Sci. USA* **2004**, *101*, 5732.

(4) Kawasaki, T.; Suzuki, K.; Hakoda, Y.; Soai, K. *Angew. Chem. Int. Ed.* **2008**, *47*, 496.

(5) Bag, B. G.; von Kiedrowski, G. *Pure Appl. Chem.* **1996**, *68*, 2145.

(6) Cleaves, H. J. *J. Theor. Biol.* **2010**, *263*, 490.

(7) Freeman, F. *Rev. React. Species Chem. React.* **1976**, *1*, 179.

(8) Jaky, M.; Szammer, J.; Simon-Trompler, E. *Int. J. Chem. Kinet.* **2006**, *38*, 444.

(9) Ameta, S. C.; Pande, P. N.; Gupta, H. L.; Chowdhry, H. C. *Acta Phys. Chem.* **1980**, *26*, 89.

(10) Ameta, S. C.; Gupta, H. L.; Pande, P. N.; Chaudhary, H. C. *Z. Phys. Chem. Leipzig* **1980**, *261*, 802.

(11) Ameta, S. C.; Pande, P. N.; Gupta, H. L.; Chowdhry, H. C. *Z. Phys. Chem. Leipzig* **1980**, *261*, 1222.

(12) Ameta, S. C.; Pande, P. N.; Gupta, H. L.; Chowdhry, H. C. *Acta Chim. Acad. Sci. Hung.* **1982**, *110*, 7.

(13) Hassan, R. M.; Mousa, M. A.; Wahdan, M. H. *J. Chem. Soc. Dalton Trans.* **1988**, 605.

(14) Andres-Ordax, F. J.; Arrizabalaga, A.; Peche, R.; Quintana, M. A. *An. Quim.* **1991**, *87*, 828.

(15) Andres-Ordax, F. J.; Arrizabalaga, A.; Casado, J.; Peche, R. *React. Kinet. Catal. Lett.* **1991**, *44*, 293.

(16) Hassan, R. M. *Can. J. Chem.* **1991**, *69*, 2018.

(17) Andres-Ordax, F. J.; Arrizabalaga, A.; Peche, R.; Quintana, M. A. *An. Quim.* **1992**, *88*, 440.

(18) Insausti, M. J.; Mata-Perez, F.; Alvarez-Macho, M. P. *Collect. Czech. Chem. Commun.* **1994**, *59*, 528.

(19) Insausti, M. J.; Mata-Perez, F.; Alvarez-Macho, M. P. *Int. J. Chem. Kinet.* **1995**, *27*, 507.

(20) Insausti, M. J.; Mata-Perez, F.; Alvarez-Macho, M. P. *Collect. Czech. Chem. Commun.* **1996**, *61*, 232.

(21) Arrizabalaga, A.; Andres-Ordax, F. J.; Fernandez-Aranguiz, M. Y.; Peche, R. *Int. J. Chem. Kinet.* **1996**, *28*, 799.

(22) Iloukhani, H.; Bahrami, H.; *Int. J. Chem. Kinet.* **1999**, *31*, 95.

(23) Iloukhani, H.; Moazenzadeh, M.; *Phys. Chem. Liq.* **2001**, *39*, 429.

(24) Khan, F. H.; Ahmad, F. *Oxid. Commun.* **2004**, *27*, 869.

(25) Bahrami, H.; Zahedi, M. *Can. J. Chem.* **2004**, *82*, 430.

(26) Zahedi, M.; Bahrami, H. *Kinet. Catal.* **2004**, *45*, 351.

(27) Andres-Ordax, F. J.; Arrizabalaga, A.; Martinez, J. I. *An. Quim.* **1984**, *80*, 531.

(28) Garrido, J. A.; Perez-Benito, J. F.; Rodríguez, R. M.; De Andres, J.; Brillas, E. *J. Chem. Res. (S)* **1987**, 380.

(29) Brillas, E.; Garrido, J. A.; Perez-Benito, J. F.; Rodríguez, R. M.; De Andres, J. *Collect. Czech. Chem. Commun.* **1988**, *53*, 479.

(30) De Andres, J.; Brillas, E.; Garrido, J. A.; Perez-Benito, J. F.; Rodríguez, R. M. *Gazz. Chim. Ital.* **1988**, *118*, 203.

(31) De Andres, J.; Brillas, E.; Garrido, J. A.; Perez-Benito, J. F. *J. Chem. Soc. Perkin Trans. 2* **1988**, 107.

(32) Rodríguez, R. M.; De Andres, J.; Brillas, E.; Garrido, J. A.; Perez-Benito, J. F. *New J. Chem.* **1988**, *12*, 143.

(33) Andres-Ordax, F. J.; Arrizabalaga, A.; Ortega, K. *An. Quim.* **1989**, *85*, 218.

(34) Perez-Benito, J. F.; Rodríguez, R. M.; De Andres, J.; Brillas, E.; Garrido, J. A. *Int. J. Chem. Kinet.* **1989**, *21*, 71.

(35) Insausti, M. J.; Mata-Perez, F.; Alvarez-Macho, M. P. *An. Quim.* **1990**, *86*, 710.

(36) Insausti, M. J.; Mata-Perez, F.; Alvarez-Macho, M. P. *An. Quim.* **1991**, *87*, 821.

(37) Insausti, M. J.; Mata-Perez, F.; Alvarez-Macho, M. P. *An. Quim.* **1991**, *87*, 877.

(38) Insausti, M. J.; Mata-Perez, F.; Alvarez-Macho, M. P. *Int. J. Chem. Kinet.* **1991**, *23*, 593.

(39) Insausti, M. J.; Mata-Perez, F.; Alvarez-Macho, M. P. *Collect. Czech. Chem. Commun.* **1992**, *57*, 2331.

(40) Insausti, M. J.; Mata-Perez, F.; Alvarez-Macho, M. P. *Int. J. Chem. Kinet.* **1992**, *24*, 411.

(41) Insausti, M. J.; Mata-Perez, F.; Alvarez-Macho, M. P. *React. Kinet. Catal. Lett.* **1993**, *51*, 51.

(42) Li, H. X.; Huang, X. J.; Deng, J. F. *Chem. Phys.* **1996**, *208*, 229.

(43) Bahrami, H.; Zahedi, M. *Int. J. Chem. Kinet.* **2006**, *38*, 1.

(44) Bahrami, H.; Zahedi, M. *J. Iran. Chem. Soc.* **2008**, *5*, 535.

(45) Bahrami, H.; Davari, M. D.; Keshavari, M.; Zahedi, M.; Bazgir, A.; Moosavi-Movahedi, A. A. *Int. J. Chem. Kinet.* **2009**, *41*, 689.

(46) Khatti, Z.; Davari, M. D.; Bahrami, H.; Zahedi, M. *Prog. React. Kinet. Mech.* **2010**, *35*, 1.

(47) Wiberg, K. B.; Freeman, F. *J. Org. Chem.* **2000**, *65*, 573.

(48) Jaky, M.; Simon-Trompler, E. *Int. J. Chem. Kinet.* **2002**, *34*, 561.

(49) Kovacs, K. A.; Grof, P.; Burai, L.; Riedel, M. *J. Phys. Chem. A* **2004**, *108*, 11026.

(50) Perez-Benito, J. F. *J. Phys. Chem. C* **2009**, *113*, 15982.

(51) Jiang, J.; Pang, S. Y.; Ma, J. *Environ. Sci. Technol.* **2009**, *43*, 8326.

(52) Jiang, J.; Pang, S. Y.; Ma, J. *Environ. Sci. Technol.* **2010**, *44*, 4270.

(53) Verma, R. S.; Reddy, M. J.; Shastry, V. R. *J. Chem. Soc., Perkin Trans. 2* **1976**, 469.

(54) Arrizabalaga, A.; Andres-Ordax, F. J.; Fernandez-Aranguiz, M. Y.; Peche, R. *Int. J. Chem. Kinet.* **1997**, *29*, 181.

(55) Mata-Perez, F.; Perez-Benito, J. F. *J. Chem. Educ.* **1987**, *64*, 925.

(56) Coetzee, J. F.; Ritchie, C. D. *Solute-Solvent Interactions*; Dekker: New York, 1969; p 17.

(57) Insausti, M. J.; Mata-Perez, F.; Alvarez-Macho, M. P. *Collect. Czech. Chem. Commun.* **1992**, *57*, 2331.

(58) Perez-Benito, J. F.; Mata-Perez, F.; Brillas, E. *Can. J. Chem.* **1987**, *65*, 2329.

(59) Barrow, G. M. *Physical Chemistry*; McGraw-Hill: New York, 1966; p 803.

(60) Perez-Benito, J. F.; Arias, C. *J. Colloid Interface Sci.* **1992**, *152*, 70.

(61) Wells, C. F.; Davies, G. *J. Chem. Soc. A* **1967**, 1858.

(62) Morgan, J. J.; Stumm, W. *J. Colloid Sci.* **1964**, *19*, 347.

(63) Wiberg, K. B. *Physical Organic Chemistry*; Wiley: New York, 1964; p 379.

(64) Krug, R. R.; Hunter, W. G.; Grieger, R. A. *Nature* **1976**, *261*, 566.

(65) Sharp, K. *Protein Sci.* **2001**, *10*, 661.

(66) Cornish-Bowden, A. *J. Biosci.* **2002**, *27*, 121.

(67) Starikov, E. B.; Norden, B. *J. Phys. Chem. B* **2007**, *111*, 14431.

(68) Krug, R. R.; Hunter, W. G.; Grieger, R. A. *J. Phys. Chem.* **1976**, *80*, 2335.

(69) Krug, R. R.; Hunter, W. G.; Grieger, R. A. *J. Phys. Chem.* **1976**, *80*, 2341.

(70) Perez-Benito, J. F. *Chem. Scr.* **1987**, *27*, 433.

(71) Linert, W.; Jameson, R. F. *Chem. Soc. Rev.* **1989**, *18*, 477.

(72) Linert, W. *Chem. Soc. Rev.* **1994**, *23*, 429.

(73) Qian, H. *J. Chem. Phys.* **1998**, *109*, 10015.

(74) Rooney, J. J. *J. Mol. Catal. A* **1998**, *129*, 131.

(75) Plonka, A. *J. Mol. Struct.* **1999**, *479*, 177.

(76) Plonka, A. *Prog. React. Kinet. Mech.* **2000**, *25*, 109.

(77) Cooper, A.; Johnson, C. M.; Lakey, J. H.; Nollmann, M. *Biophys. Chem.* **2001**, *93*, 215.

(78) Liu, L.; Guo, Q. X. *Chem. Rev.* **2001**, *101*, 673.

TABLE 1: Symbols and Side Chains of the α-Amino Acids Studied[a]

α-amino acid	symbol	side chain (R)
glycine	Gly	H
L-alanine	Ala	CH_3
L-threonine	Thr	$CHOH - CH_3$
L-valine	Val	$CH(CH_3) - CH_3$
L-glutamic acid	Glu	$CH_2 - CH_2 - CO_2H$
L-leucine	Leu	$CH_2 - CH(CH_3) - CH_3$
L-isoleucine	Ile	$CH(CH_3) - CH_2 - CH_3$

[a] General formula: $H_2N - CHR - CO_2H$.

TABLE 2: Rate Constants for the Non-Autocatalytic and Autocatalytic Reaction Pathways in the Permanganate Oxidation of L-Threonine [a]

Method	k_1 [b] / 10^{-5} s^{-1}	k_2 [c] / M^{-1} s^{-1}
Differential	1.34 ± 0.07	0.175 ± 0.013
Integrated[d]	1.28 ± 0.05	0.181 ± 0.011

[a] $[MnO_4^-]_o = 8.00 \times 10^{-4}$ M, [L-threonine] = 1.08×10^{-2} M, $[KH_2PO_4] = 9.60 \times 10^{-2}$ M, $[K_2HPO_4] = 4.80 \times 10^{-2}$ M, pH = 6.52, T = 25.0 °C. [b] Rate constant for the non-autocatalytic reaction pathway. [c] Rate constant for the autocatalytic reaction pathway.

TABLE 3: Rate and Equilibrium Constants for the Non-Autocatalytic and Autocatalytic Reaction Pathways Associated to the Effect of pH on the Kinetics of the Permanganate Oxidation of L-Threonine [a]

Constant	Non-Autocatalytic	Autocatalytic
k_a [b]	$(9.85 \pm 0.82) \times 10^{-4}$ M^{-1} s^{-1}	2.07 ± 0.68 M^{-2} s^{-1}
k_b [c]	$(1.86 \pm 0.16) \times 10^{-2}$ M^{-1} s^{-1}	391 ± 8 M^{-2} s^{-1}
K_a [d]	$(6.29 \pm 0.53) \times 10^{-9}$ M	$(1.05 \pm 0.02) \times 10^{-8}$ M
pK_a	8.20 ± 0.04	7.98 ± 0.01

[a] $[MnO_4^-]_o = 8.00 \times 10^{-4}$ M, [L-threonine] $= 1.08 \times 10^{-2}$ M, $[KH_2PO_4] + [K_2HPO_4] =$ 0.144 M, pH = 6.13-7.53, $T = 25.0$ °C. [b] Rate constant for the acid-catalyzed reaction pathway. [c] Rate constant for the base-catalyzed reaction pathway. [d] Equilibrium acidity constant for the dissociation of the α-amino acid.

TABLE 4: Standard Activation Enthalpies and Entropies for the Non-Autocatalytic and Autocatalytic Reaction Pathways in the Permanganate Oxidation of α-Amino Acids[a,b,c]

α-amino acid	$\Delta H^{o}_{\neq 1}$/kJ mol^{-1}	$\Delta S^{o}_{\neq 1}$/J K^{-1} mol^{-1}	$\Delta H^{o}_{\neq 2}$/kJ mol^{-1}	$\Delta S^{o}_{\neq 2}$/J K^{-1} mol^{-1}
glycine	69.3 ± 4.1	- 82 ± 14	57.4 ± 2.8	- 32 ± 9
L-alanine	71.5 ± 2.2	- 80 ± 7	64.6 ± 4.3	- 24 ± 14
L-threonine	44.4 ± 1.2	- 149 ± 4	67.9 ± 0.6	13 ± 2
L-valine	66.7 ± 2.3	- 90 ± 7	101.8 ± 2.2	87 ± 7
L-glutamic acid	60.3 ± 1.8	- 114 ± 6	78.3 ± 1.1	24 ± 4
L-leucine	64.3 ± 2.8	- 94 ± 9	93.4 ± 3.0	66 ± 10
L-isoleucine	66.9 ± 2.5	- 90 ± 8	97.9 ± 1.7	76 ± 6

[a] $[MnO_4^-] = 5.00 \times 10^{-4}$ M, $[NH_3^+CHRCO_2^-] = (2.16 - 8.00) \times 10^{-2}$ M, pH = 6.78, T = 25.0 - 45.0 ºC. [b] The activation energies can be calculated as: $E_a = \Delta H^{o}_{\neq} + 2.6$ kJ mol^{-1}. [c] The activation entropies are referred to the 1-M standard state.

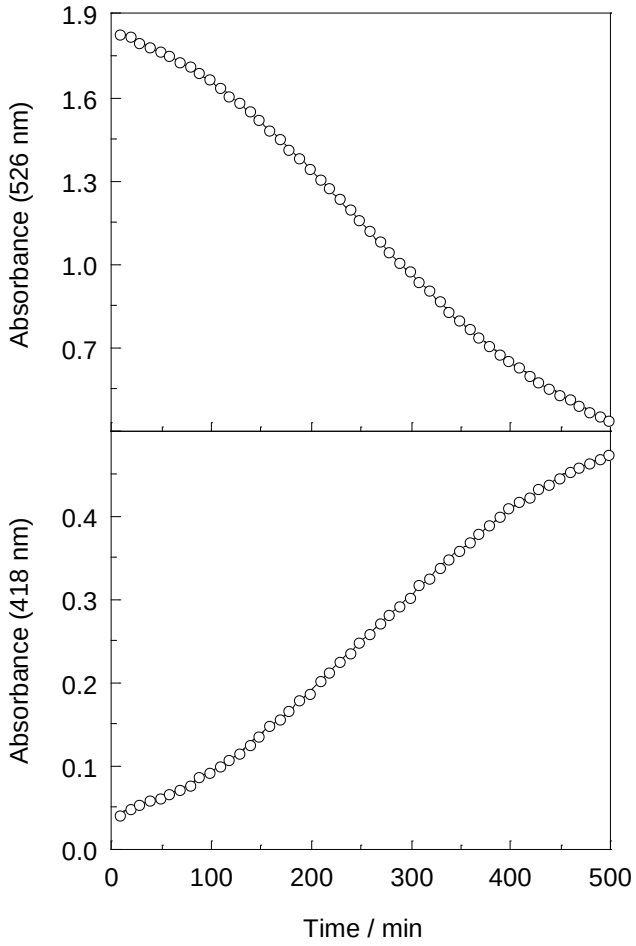

Figure 1. Dependencies of the absorbances at 418 (bottom) and 526 (top) nm on time for the reaction of $KMnO_4$ (8.00×10^{-4} M) with L-threonine (1.08×10^{-2} M) in the presence of KH_2PO_4 (9.60×10^{-2} M) - K_2HPO_4 (4.80×10^{-2} M) buffer at pH 6.52 and 25.0 ºC.

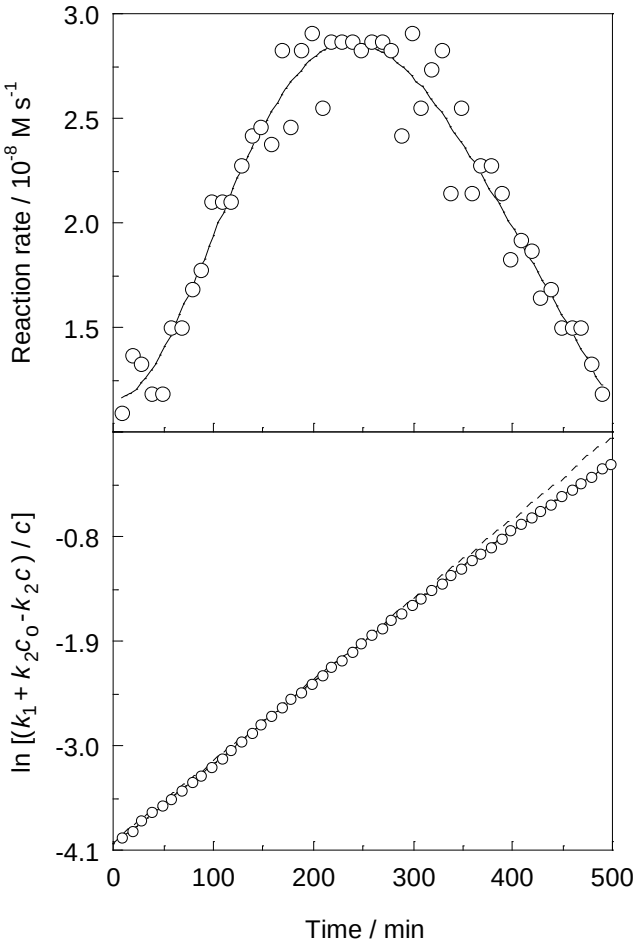

Figure 2. Dependencies of the reaction rate (top) and of ln $[(k_1 + k_2\, c_o - k_2\, c) / c]$ (bottom) on time for the reaction of $KMnO_4$ (8.00×10^{-4} M) with L-threonine (1.08×10^{-2} M) in the presence of KH_2PO_4 (9.60×10^{-2} M) - K_2HPO_4 (4.80×10^{-2} M) buffer at pH 6.52 and 25.0 ºC.

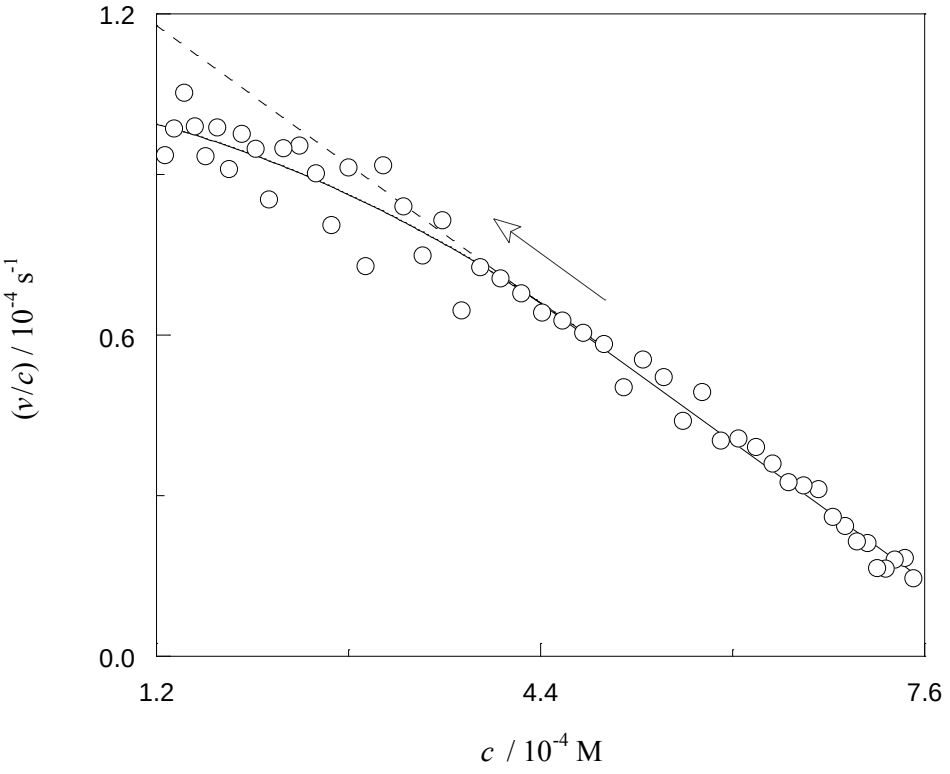

Figure 3. Dependence of the *v*/*c* ratio on the permanganate concentration for the reaction of $KMnO_4$ (8.00×10^{-4} M) with L-threonine (1.08×10^{-2} M) in the presence of KH_2PO_4 (9.60×10^{-2} M) - K_2HPO_4 (4.80×10^{-2} M) buffer at pH 6.52 and 25.0 ºC. The arrow indicates the progression of the reaction.

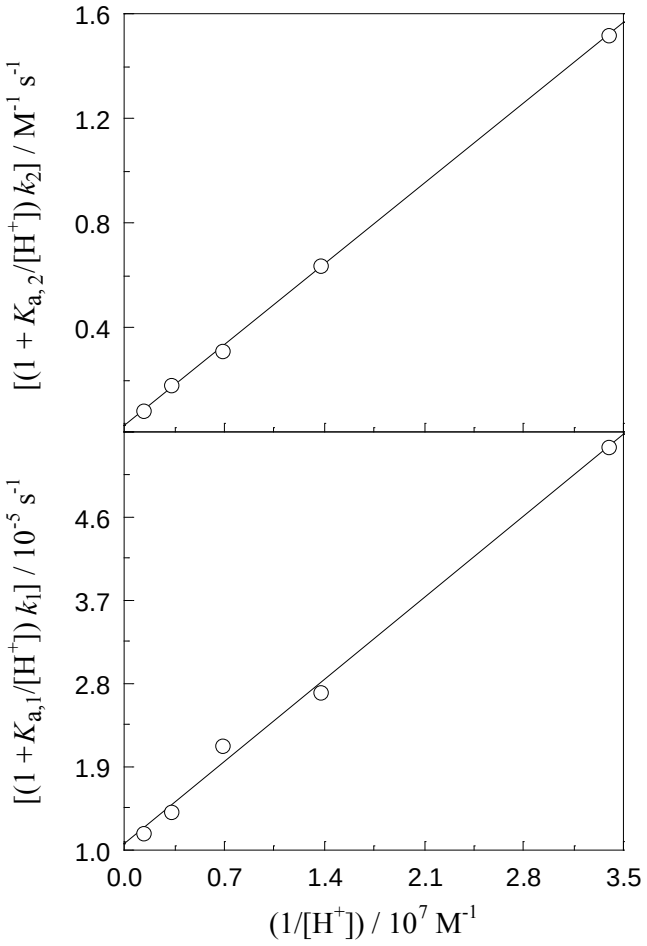

Figure 4. Dependencies of $(1 + K_{a,1}/[H^+])\ k_1$ (bottom) and $(1 + K_{a,2}/[H^+])\ k_2$ (top) on $1/[H^+]$ for the reaction of $KMnO_4$ (8.00×10^{-4} M) with L-threonine (1.08×10^{-2} M) in the presence of phosphate buffer ($[KH_2PO_4] + [K_2HPO_4] = 0.144$ M) at pH 6.13-7.53 and 25.0 ºC.

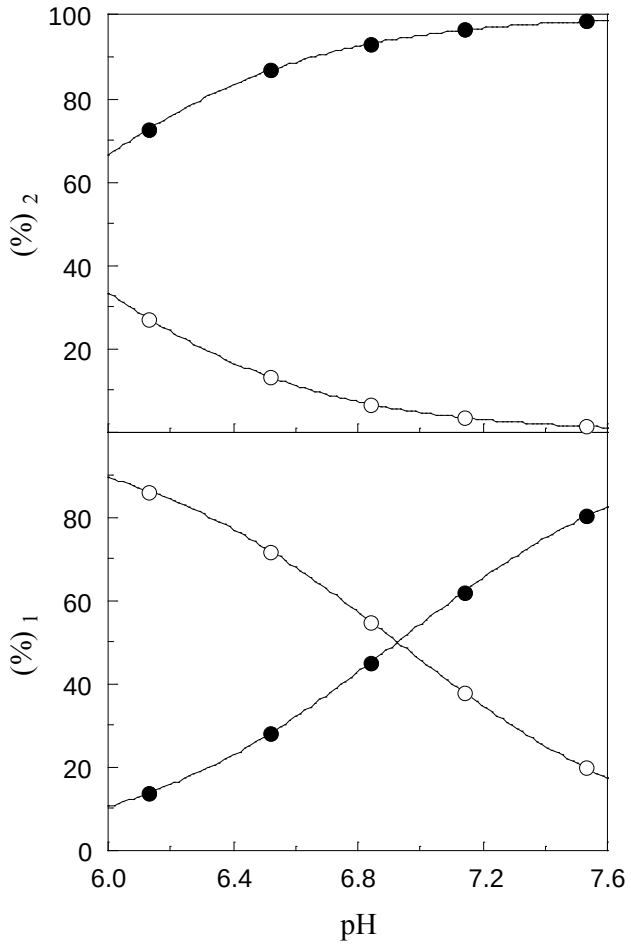

Figure 5. Dependencies of the relative contributions for the acid-catalyzed (empty points) and the base-catalyzed (filled points) pathways of the non-autocatalytic (bottom) and the autocatalytic (top) reactions on the pH for the reduction of $KMnO_4$ (8.00×10^{-4} M) with L-threonine (1.08×10^{-2} M) in the presence of phosphate buffer ($[KH_2PO_4] + [K_2HPO_4] = 0.144$ M) at 25.0 ºC.

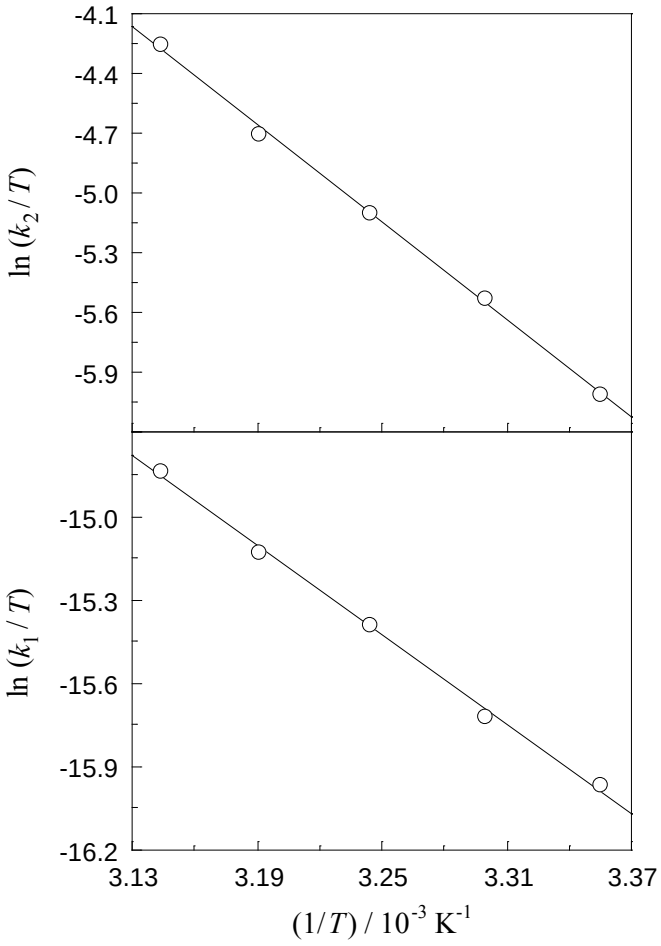

Figure 6. Eyring plots for the non-autocatalytic (bottom) and autocatalytic (top) pathways in the reaction of $KMnO_4$ (5.00×10^{-4} M) with L-threonine (2.16×10^{-2} M) at pH 6.78 in the temperature range 25.0- 45.0 ºC.

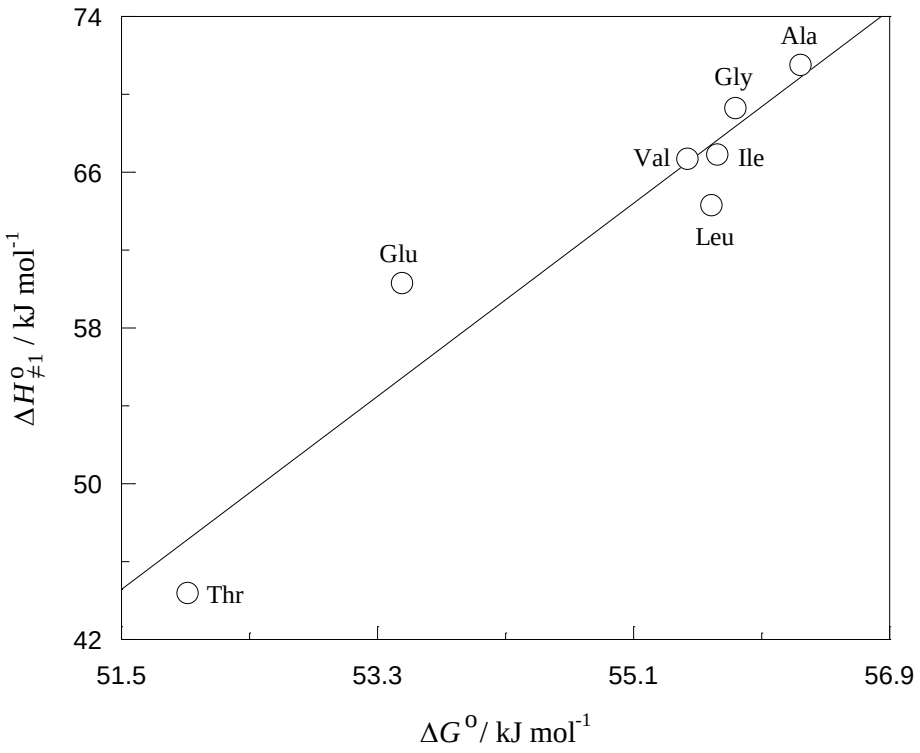

Figure 7. Dependence of the standard activation enthalpies of the non-autocatalytic pathway for the reactions of $KMnO_4$ with seven α-amino acids on the standard Gibbs energy for the dissociation of the protonated amino group of the corresponding α-amino acid (r = 0.9558, P = 0.0006).

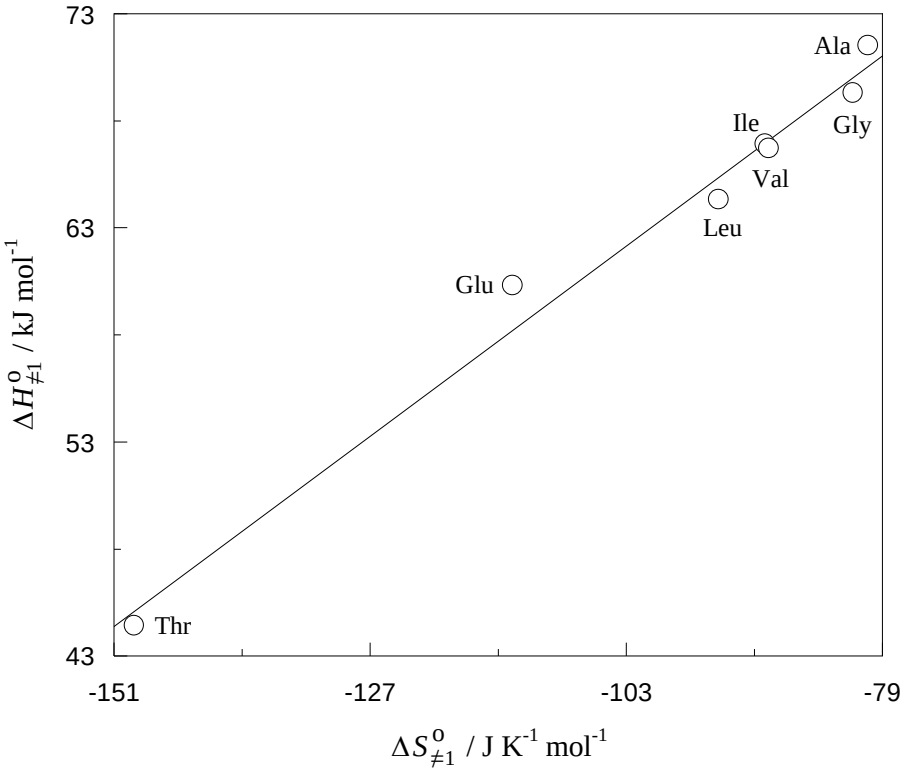

Figure 8. Enthalpy-entropy correlation for the non-autocatalytic pathway in the reactions of $KMnO_4$ with seven α-amino acids (T_{iso} = 370 ± 21 K, r = 0.9923, P = 0.00008).

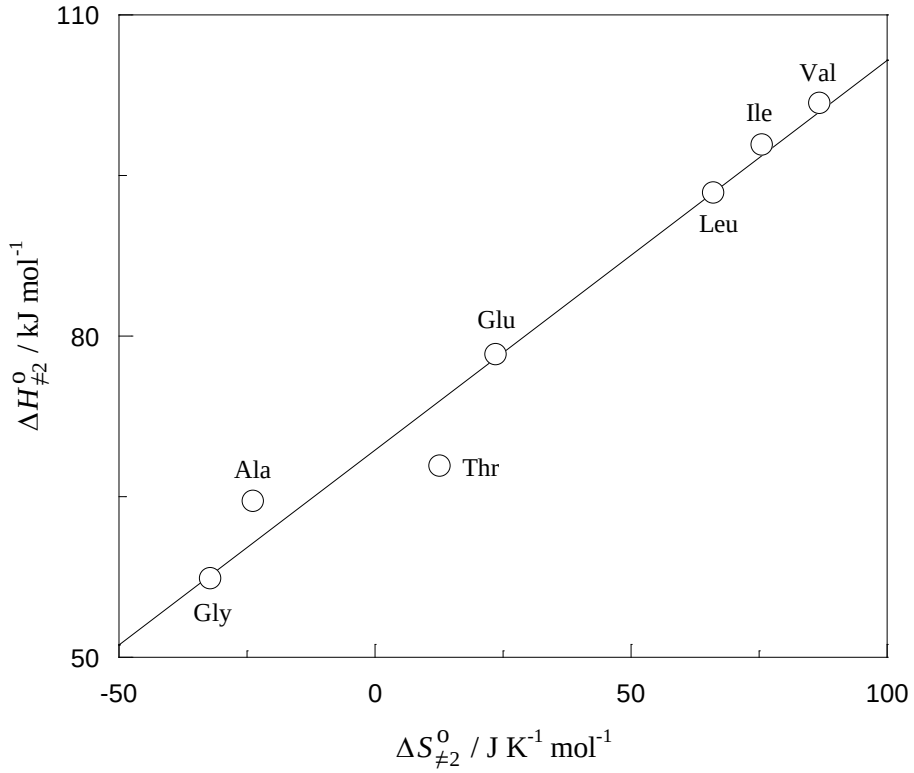

Figure 9. Enthalpy-entropy correlation for the autocatalytic pathway in the reactions of $KMnO_4$ with seven α-amino acids (T_{iso} = 364 ± 28 K, r = 0.9855, P = 0.0002).

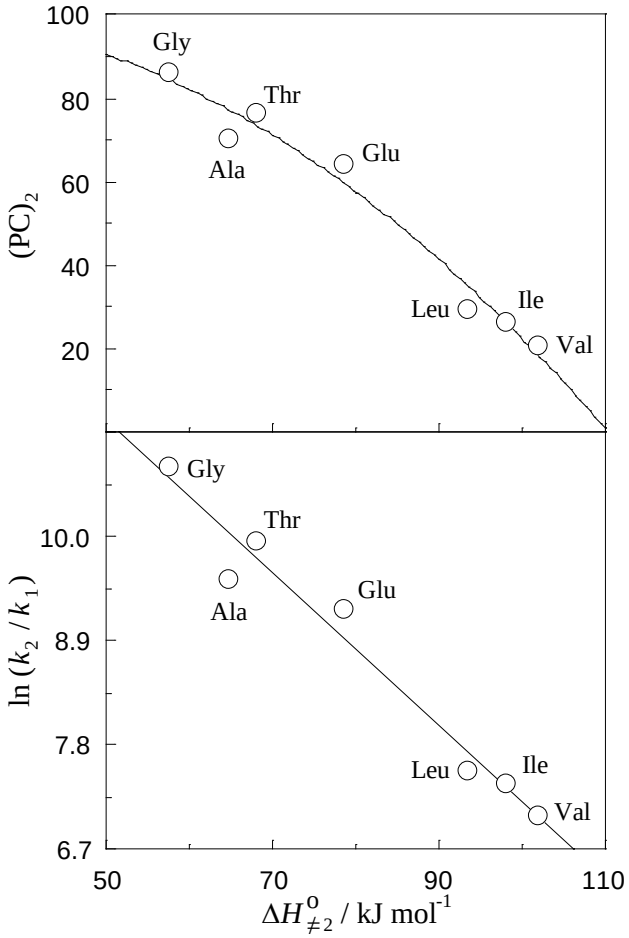

Figure 10. Dependencies of the logarithm of the ratio between the rate constants of the autocatalytic and non-autocatalytic pathways (bottom, r = 0.9840, P = 0.0002) and the percentage of the overall reaction corresponding to the autocatalytic pathway (top, r = 0.9865, P = 0.0002) on the standard activation enthalpy of the autocatalytic pathway for the reactions of $KMnO_4$ (5.00×10^{-4} M) with seven α-amino acids (5.08×10^{-2} M) at pH 6.78 and 25.0 ºC. The curve represents the best fit to a second-degree polynomial.

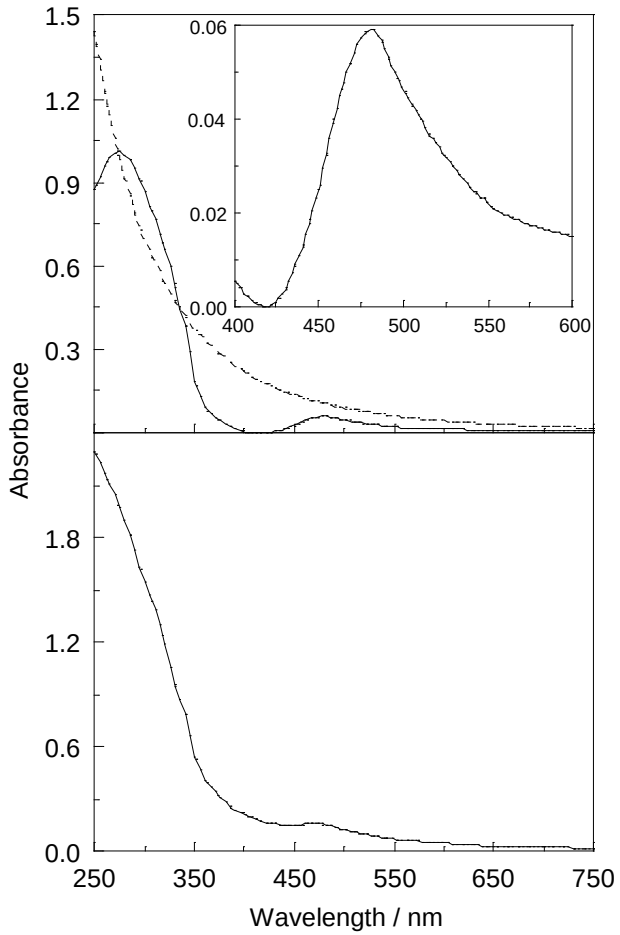

Figure 11. UV-vis sprectrum of the product from the reduction of $KMnO_4$ (4.00×10^{-4} M) by glycine (0.130 M) in the presence of KH_2PO_4 (0.120 M) - K_2HPO_4 (0.120 M) buffer at pH 6.61 and 25.0 ºC (bottom), and the corresponding contributions from light absorption (top, continuous line) and light scattering (top, dashed line). Inset: Detail showing the peak of Mn(III) at 480 nm.

“Table of Contents” Graphic